Interpreting GEMS geostationary satellite observations of the diurnal variation of nitrogen dioxide (NO2) over East Asia

Laura Hyesung Yang[1], Daniel J. Jacob[1,2], Ruijun Dang[1], Yujin J. Oak[1], Haipeng Lin[1], Jhoon Kim[3], Shixian Zhai[4], Nadia K. Colombi[2], Drew C. Pendergrass[1], Ellie Beaudry[1], Viral Shah[5], Xu Feng[1], Robert M. Yantosca[1], Heesung Chong[6], Junsung Park[7], Hanlim Lee[7], Won-Jin Lee[8], Soontae Kim[9], Eunhye Kim[9], Katherine R. Travis[10], James H. Crawford[10], Hong Liao[11]

[1] Harvard University, John A. Paulson School of Engineering and Applied Sciences, Cambridge, MA 02138, USA
[2] Harvard University, Department of Earth and Planetary Sciences, Cambridge, MA 01238, USA
[3] Yonsei University, Department of Atmospheric Sciences, Seoul 03722, South Korea
[4] Earth and Environmental Sciences Programme and Graduation Division of Earth and Atmospheric Sciences, Faculty of Science, The Chinese University of Hong Kong, Sha Tin, Hong Kong SAR, China
[5] Global Modeling and Assimilation Office, NASA Goddard Space Flight Center, Greenbelt, MD 20771, USA, and Science Systems and Applications, Inc., Lanham, MD 20706, USA
[6] Center for Astrophysics | Harvard & Smithsonian, Cambridge, Massachusetts 02138, USA
[7] Pukyong National University, Division of Earth Environmental System Science, Busan 48513, South Korea
[8] Environmental Satellite Center, National Institute of Environmental Research, Incheon 22689, South Korea
[9] Ajou University, Department of Environmental and Safety Engineering, Suwon 16499, South Korea
[10] NASA Langley Research Center, Hampton, VA 23666, USA
[11] Collaborative Innovation Center of Atmospheric Environment and Equipment Technology/Joint International Research Laboratory of Climate and Environment Change, School of Environmental Science and Engineering, Nanjing University of Information Science and Technology, Nanjing 210044, China

Correspondence to: Laura Hyesung Yang (laurayang@g.harvard.edu)

Abstract. Nitrogen oxide radicals ($NO_x \equiv NO + NO_2$) emitted by fuel combustion are important precursors of ozone and particulate matter pollution, and NO_2 itself is harmful to public health. The Geostationary Environment Monitoring Spectrometer (GEMS), launched in space in 2020, now provides hourly daytime observations of NO_2 columns over East Asia. This diurnal variation offers unique information on the emission and chemistry of NO_x, but it needs to be carefully interpreted. Here we investigate the drivers of the diurnal variation of NO_2 observed by GEMS during winter and summer over Beijing and Seoul. We place the GEMS observations in the context of ground-based column observations (Pandora instruments) and GEOS-Chem chemical transport model simulations. We find good agreement between the diurnal variations of NO_2 columns in GEMS, Pandora, and GEOS-Chem, and we use GEOS-Chem to interpret these variations. NO_x emissions are four times higher in the daytime than at night, driving an accumulation of NO_2 over the course of the day, offset by losses from chemistry and transport (horizontal flux divergence). For the urban core, where the Pandora instruments are located, we find that NO_2 in winter increases throughout the day due to high daytime emissions and increasing NO_2/NO_x ratio from

40 entrainment of ozone, partly balanced by loss from transport and with negligible role of chemistry. In summer, by contrast, chemical loss combined with transport drives a minimum in the NO_2 column at 13-14 local time. Segregation of the GEMS data by wind speed further demonstrates the effect of transport, with NO_2 in winter accumulating throughout the day at low winds but flat at high winds. The effect of transport can be minimized in summer by spatially averaging observations over the broader metropolitan scale, under

45 which conditions the diurnal variation of NO_2 reflects a dynamic balance between emission and chemical loss.

1. Introduction

The Geostationary Environment Monitoring Spectrometer (GEMS) satellite instrument was launched in February 2020 by the National Institute of Environmental Research (NIER) to observe air quality over

50 East Asia. GEMS is the first geostationary instrument directed at air quality and provides hourly column measurements of several gases including nitrogen dioxide (NO_2) (J. Kim et al., 2020). NO_2 is part of the nitrogen oxides ($NO_x \equiv NO + NO_2$) radical family, which is emitted by fuel combustion and whose chemistry plays a critical role in driving ozone (O_3) and fine particulate matter ($PM_{2.5}$) formation. NO_2 itself is of concern as an air pollutant. Loss of NO_x is by atmospheric oxidation by the hydroxyl radical

55 (OH) and ozone, resulting in a lifetime of a few hours in summer and about a day in winter (Shah et al., 2020). The diurnal cycle of NO_2 measured from geostationary orbit offers unique information on the emission, chemistry, and transport of NO_x. Here we interpret the GEMS observations with the GEOS-Chem chemical transport model (CTM) to better understand the processes controlling this diurnal cycle.

Several studies have examined the diurnal variation of NO_2 in urban air using surface

60 concentrations from air quality networks. The data typically exhibit bimodal maxima in the morning around 7-9 local time (LT) and in the evening around 19-21 LT, including over Beijing and Seoul (Cheng et al., 2018; H. Kim et al., 2020). This has been commonly attributed to high NO_x emission during morning and evening rush hours (Kendrick et al., 2015; Cheng et al., 2018), but urban NO_x emission inventories show little variation during daytime (Miao et al., 2020). Moutinho et al. (2020) found that the morning and

65 evening NO_2 maxima could be driven by shallow mixing depths, in contrast to the middle of the day where

surface heating drives deep mixing and defines the depth of the planetary boundary layer (PBL) in daily

contact with the surface. The PBL depth extends typically to 1-3 km altitude.

Ground-based measurements of NO_2 columns are available from the Pandora Sun-staring

spectrometer instrument network used for validating satellite observations (Herman et al., 2009; Kanaya et

70 al., 2014; Judd et al., 2020; Verhoelst et al., 2021). Column measurements integrate concentrations from

the surface to the top of the atmosphere and are therefore not directly sensitive to mixing depth. The

Pandora network consists mainly of urban sites, where the NO_2 column and its variability are mainly within

the PBL (Yang et al., 2023). The Pandora data from Seoul tend to show an increasing trend in the early

morning followed by flat concentrations over the rest of the daytime, with less diurnal variation than NO_2

75 concentrations in surface air (Crawford et al., 2021). Nearby sites can show different diurnal variations,

pointing to a major role of local transport in driving this variation (Chang et al., 2022; S. Kim et al., 2023).

Satellite observations of NO_2 from polar sun-synchronous low-earth orbit (LEO) have been made

since 1995 starting with the GOME instrument (Martin et al., 2002) but observe by design at a single time

of day. Several studies have combined observations from the SCIAMACHY or GOME-2 instruments

80 observing in the morning at 9-10 LT and the OMI instrument observing in the afternoon at 13-14 LT to get

some information on NO_2 diurnal variation. Boersma et al. (2008) found decreases from morning to

afternoon over urban regions that they attributed to photochemical loss, and increases from morning to

afternoon over tropical biomass burning regions that they attributed to a midday maximum in emissions.

Boersma et al. (2009) found that the urban morning-to-afternoon decrease was largest in summer and

85 absent in winter. Penn and Holloway (2020) found that NO_2 column ratios between morning and afternoon

were lower than surface NO_2 concentration ratios, as would be expected from deeper vertical mixing in the

afternoon. Ghude et al. (2020) found an important role for transport in driving morning-to-afternoon

variations in NO_2 columns over urban India.

Here we analyze and compare the NO_2 diurnal cycles observed by GEMS over the Seoul and Beijing metropolitan areas in winter and summer. We compare to the diurnal cycles observed by Pandora in the urban cores and to simulations with the GEOS-Chem CTM. We use GEOS-Chem to separate and quantify the roles of emission, chemistry, and transport in driving the NO_2 diurnal cycles observed from GEMS over different spatial scales. This work provides a basis for more quantitative application of GEMS observations as top-down information on NO_x emissions, and more generally for interpreting the diurnal cycle of NO_2 from geostationary orbit with application to the TEMPO instrument over North America launched in April 2023 (Zoogman et al., 2017) and the Sentinel-4 instrument over Europe to be launched in 2024 (Gulde et al., 2017).

2. Observations and model

2.1 GEMS data

GEMS is an ultraviolet-visible instrument measuring back-scattered solar spectra at $300 - 500$ nm (J. Kim et al., 2020). It was launched in February 2020 in geostationary orbit at a longitude of 128.25°E. Its native pixel resolution is 3.5×8 km^2 at Seoul, with variations in Level 2 product resolutions depending on the pixel binning configurations. We use hourly total NO_2 slant column density from the GEMS L2 NO_2 version 2.0 product at 3.5×8 km^2 resolution for December-February (DJF) 2021/22 and June-August (JJA) 2022 (NIER, 2023). The GEMS NO_2 algorithm uses differential optical absorption spectroscopy (DOAS) to fit back-scattered solar spectra within the $432 - 450$ nm range (J. Kim et al., 2020). This yields the slant column density along the light path (L2 data). We use all GEMS L2 NO_2 version 2.0 data that pass algorithm quality flag ≤ 112, final algorithm flag ≤ 1, solar zenith angle (SZA) < 70°, viewing zenith angle (VZA) < 70°, and cloud fraction < 0.3 (Lee et al., 2020).

The vertical column density of NO_2 is obtained by dividing the slant column density by an air mass factor (AMF) characterizing the photon path from the Sun down through the atmosphere and back up to the instrument. The AMF depends on the viewing geometry and on the scattering properties of the atmosphere:

$$AMF = AMF_G \int_0^\infty w(z)S(z)dz \qquad (1)$$

where AMF_G is the geometric AMF defined by the solar zenith angle (SZA) and the satellite viewing angle (VZA), $w(z)$ is the scattering weight that defines the instrument's sensitivity to NO_2 at altitude z, and $S(z)$ is a normalized vertical profile of NO_2 number density called the shape factor (Palmer et al., 2001). Scattering weights are calculated with a radiative transfer model and typically increase with altitude (Martin et al., 2002). The shape factor is usually estimated with a CTM.

Here we use scattering weights at 448 nm calculated for the application to a 435 – 461 nm spectral window compiled as a look-up table dependent on SZA, VZA, relative azimuth angle (RAA), surface albedo, cloud top pressure, and effective cloud fraction (R. Park and Kwon, 2020). We specify the shape factor with local NO_2 concentrations from the GEOS-Chem simulation described in Section 2.3. In simulations of observations from the KORUS-AQ aircraft campaign over Seoul, Yang et al. (2023) showed that GEOS-Chem was successful in reproducing the observed diurnal variation in the vertical profile of NO_2 as driven by PBL mixing, with important implications for the diurnal variation in the AMF. The GEOS-Chem simulation extends vertically to the mesosphere, and we compute in this manner the AMF for the whole atmosphere to obtain a total vertical column density. The contribution of the stratosphere to the total NO_2 column in GEOS-Chem is only 9- 20% for the Seoul and Beijing metropolitan areas of interest here. The PBL extending to 2 km altitude accounts for 95% of the tropospheric column over the Seoul Metropolitan Area (Yang et al., 2023).

2.2 Pandora data

The Pandora instruments measure radiance at 280 – 525 nm (Herman et al., 2018) and fit total column NO_2 (including the stratosphere). There are two Pandora sites in Seoul and one in Beijing (40.0°N, 116.4°E; O. Liu et al., 2023) for the 2021-2022 period. The two Pandora sites in Seoul are at Seoul National University (Seoul – SNU; 37.5°N, 127.0°E) in the southern part of Seoul (M. Kim et al., 2021; S. Park et al., 2018) and at Yonsei University (Seoul – YSU; 37.6°N, 126.9°E) in the northern part of Seoul (J. Kim., 2017). We obtain the Pandora direct Sun data from the Pandonia global network (PGN, 2023) and exclude data with a NO_2 flag of 12.

2.3 GEOS-Chem model

140   We use GEOS-Chem CTM version 13.3.4 (https://doi.org/10.5281/zenodo.5764874) driven by

assimilated meteorological data from the Goddard Earth Observing System – Forward Processing (GEOS-

FP) with a horizontal resolution of $0.25° \times 0.3125°$ ($\approx 25 \times 25$ km^2) over East Asia (24 – 52°N, 104 –

133°E) and 3-hourly boundary conditions from a global GEOS-Chem simulation with $4° \times 5°$ resolution.

The model has 47 vertical levels including 14 vertical levels in the lower 2 km. Simulations were

145   conducted for DJF 2021/2022 and JJA 2022 with 6 months of initialization for each period.

       Aside from emissions (see below), the simulation is the same as previously described by Yang et al.

(2023) and features some modifications to the standard GEOS-Chem 13.3.4 to better reproduce KORUS-

AQ aircraft observations over Korea in May-June 2016. These include aerosol nitrate photolysis, volatile

chemical product (VCP) emissions and chemistry, and reduced HO_2 uptake by aerosol. Yang et al. (2023)

150   showed that the model could successfully simulate NO_x chemistry during KORUS-AQ including the

diurnal variation of NO_2 vertical profiles affecting the diurnal variation of the AMF. This gives us

confidence in the application of GEOS-Chem normalized vertical profiles in Eq. (1) to compute AMFs for

application to the GEMS data.

       Simulations for 2022 require adjustment to NO_x emissions beyond the most recent emission

155   inventories used in GEOS-Chem for China (MEIC for 2019; Zheng et al., 2021) and Korea (KORUSv5 for

2015; Woo et al., 2020). We apply for this purpose the surface NO_2 concentration trends for China from the

Ministry of Ecology and Environment (MEE) network (MEE, 2023) and for South Korea from the

AirKorea network (KEC, 2023). Mean 2022/2019 surface NO_2 concentration ratios in China are 0.91 in

DJF and 0.83 in JJA, and mean 2022/2015 values in Korea are 0.70 in DJF and 0.51 JJA, which are applied

160   to scale the anthropogenic NO_x emissions.

       Several previous studies aside from Yang et al. (2023) have evaluated the GEOS-Chem simulation

of NO_x over East Asia. R. Park et al. (2021) found that GEOS-Chem successfully reproduced the NO_x

vertical profiles observed during KORUS-AQ. Shah et al. (2020) found a good simulation of the

seasonality of OMI NO_2 over China and its long-term trend. M. Liu et al. (2018) found that NO_2 diurnal

165   variability at the MEE stations was well captured but the model was too low, as would be expected from

the urban nature of the sites.

2.4 Diurnal variation of NO_x emissions

Figure 1 shows the diurnal cycle of NO_x emissions used by GEOS-Chem in Beijing and Seoul.

MEIC for China provides monthly NO_x emissions separately for the transportation, residential, industrial,

170   and power sectors while KORUSv5 separates mobile, area, and point sources. Neither inventory specifies

diurnal variations in emissions. In our work, we apply the diurnal pattern from X. Liu et al. (2019) for the

power sector and Miao et al. (2020) for other sources in the MEIC inventory. For KORUSv5 we apply the

diurnal pattern from X. Liu et al. (2019) for point sources, supported by results from Bae et al. (2021), and

the industrial daily pattern from Miao et al. (2020) for area sources. We estimate the diurnal variation of

175   mobile sources in KORUSv5 using hourly Seoul Transport Operation and Information Services (TOPIS,

2023) data on weekday total traffic and construction equipment activity.

Figure 1 shows that emissions are dominated by industrial and transport sources in Beijing, and by

mobile (transport) sources in Seoul. Both sectors show a broad maximum between 7 and 18 LT that defines

the overall diurnal cycle of emissions and is similar in winter and summer. There are no significant rush

180   hour peaks in transport emissions, suggesting that the surface NO_2 maxima observed in early morning and

evening are driven more by shallow mixing depths (Moutinho et al., 2020). Total NO_x emission in Beijing

in winter is 30% greater than in summer, driven by the industrial source and possibly due to workplace

heating. There is less seasonal variation in Seoul where mobile sources are the largest emitters.

3.   Intercomparison of total NO_2 columns

185   Figure 2 shows the total NO_2 columns over eastern China and South Korea observed by GEMS and

simulated by GEOS-Chem during DJF 2021/22 and JJA 2022. The GEMS data are mapped on the 0.25° ×

0.3125° GEOS-Chem grid. The yellow box delineates the Seoul Metropolitan Area (SMA). The zoomed-in

black boxes are Beijing and Seoul and the white boxes are the city centers where Pandora stations are

located. The NO$_2$ plume location in winter is shifted south due to the prevailing winds and the long NO$_x$

190   lifetime (Seo et al, 2021). We see from Figure 2 that GEMS and GEOS-Chem have consistent spatial

distributions and backgrounds, but GEOS-Chem over polluted regions is generally higher than GEMS
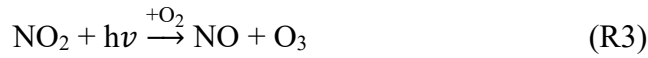
except for Seoul in winter.

Figure 3 further intercompares GEOS-Chem and GEMS using the Pandora stations in Beijing and

Seoul as evaluation metric. GEMS and GEOS-Chem reproduce the diurnal and day-to-day variability

195   observed by Pandora in DJF (R^2 = 0.87-0.90) and JJA (R^2 = 0.77-0.79). NO$_2$ column magnitudes also agree

well with Pandora in winter, with linear regression slopes of 0.94 for GEMS and 0.90 for GEOS-Chem.

Summer shows larger biases reflecting differences between the SNU and YSU Pandora sites that cannot be

resolved at the 0.25° × 0.3125° resolution of GEOS-Chem (there are few observations at the Beijing site in

JJA). YSU is more polluted than SNU, which is in a mountainous area more remote from emissions.

200   Overall, comparison to Pandora supports the diurnal and day-to-day variability seen in the GEMS and

GEOS-Chem data. The rest of our analysis focuses on the diurnal variability.

4. Diurnal variation of NO$_2$ columns on the urban scale

We start with an urban core analysis focusing on the white boxes shown in Figure 2 for Beijing and

Seoul, representing single 0.25° × 0.3125° GEOS-Chem grid cells where the Pandora stations are located.

205   Scatterplot comparisons between GEOS-Chem, GEMS, and Pandora for these grid cells were shown in

Figure 3. Figure 4 shows the diurnal variation of the total NO$_2$ column observed from GEMS and Pandora

and simulated by GEOS-Chem in Beijing. GEOS-Chem results are shown as averages for all days and for

the subset of days when GEMS observations are available (generally limited by cloud cover). Wintertime

NO$_2$ in all three datasets is flat from 10 to 11 LT and then increases from 11 to 14 LT. Summertime NO$_2$

210   decreases from 8 LT to a minimum at 13-14 LT and then increases to 16 LT, consistent between GEOS-

Chem and GEMS. Pandora observations in the summertime are too limited to show.

We used the GEOS-Chem budget tendency diagnostic to understand the drivers of the diurnal

variation in NO$_2$ columns. This diagnostic tracks the mean mass-weighted changes of column

concentrations after each model operation for any selected horizontal domain, vertical column, and time

215   period. We focus on the PBL column conservatively defined as extending to 3 km altitude after verifying

that altitudes higher than 3 km make negligible contributions to diurnal changes in the total model column.

Within the PBL column we consider the budget of NO_2 as that of NO_x ($\equiv NO + NO_2 + NO_3 + 2N_2O_5 +$

$HONO + HNO_4 + ClNO_2$) multiplied by the local NO_2/NO_x PBL column concentration ratio. This

eliminates from the budget the fast interconversion reactions within the NO_x family and provides a more

220   useful budget perspective. The NO_x family is mainly contributed by NO and NO_2, and the main

interconversion reactions defining the NO_2/NO_x ratio are

$$NO + O_3 \rightarrow NO_2 + O_2 \qquad\qquad (R1)$$
$$NO + HO_2 \rightarrow NO_2 + OH \qquad\qquad (R2)$$
$$NO_2 + h\nu \xrightarrow{+O_2} NO + O_3 \qquad\qquad (R3)$$

225   The differential net budget tendency for the PBL NO_2 column (Ω_{NO2}) can then be related to that of NO_x

(Ω_{NOx}) as

$$\left[\frac{\partial \Omega_{NO_2}}{\partial t}\right]_{net} = \alpha(t)\left[\frac{\partial \Omega_{NO_x}}{\partial t}\right]_{net} \quad (2)$$

with

$$\left[\frac{\partial \Omega_{NO_x}}{\partial t}\right]_{net} = \left[\frac{\partial \Omega_{NO_x}}{\partial t}\right]_{emission} + \left[\frac{\partial \Omega_{NO_x}}{\partial t}\right]_{chemistry} + \left[\frac{\partial \Omega_{NO_x}}{\partial t}\right]_{transport} \quad (3)$$

230   and where $\alpha(t) = \Omega_{NO_2}/\Omega_{NO_x}$ is the NO_2/NO_x PBL column ratio. The terms on the right-hand side of Eq. (3)

are updated by GEOS-Chem over its operator splitting time steps and are archived in the budget diagnostic

as spatial and temporal averages. NO_x dry deposition is included in the emission operator, but its

contribution is very small (Shah et al., 2020).

The second row of Figure 4 shows the different NO_x budget terms from Eq. (3) over hourly time

235   steps, with the net tendency as the left-hand-side term. The third row shows the NO_2/NO_x PBL column

molar ratios in GEOS-Chem. The GEOS-Chem diurnal variation in the NO_2 column in the first row reflects

the net NO_x tendency combined with the NO_2/NO_x ratio. In this manner, we see that the increase in the NO_2

column over the course of the day in winter reflects the dominant effect of daytime emissions, four times

9

higher than at night and leading to NO_x accumulation. Chemical loss is slow in winter and transport (flux

240   divergence) is the main loss term. The flat trend of the NO_2 column from 10 to 11 LT corresponds to the

diurnal minimum of the NO_2/NO_x ratio. This ratio increases over the rest of the day as the mixed layer

deepens and the freshly emitted NO is exposed to higher ozone concentrations. The increase in the ratio

contributes to the increase in the NO_2 column. The NO_2 column in GEOS-Chem thus peaks at 18 LT.

During the night, the NO_x emission decreases and the loss from transport leads to decrease in the total NO_2

245   column. The NO_2/NO_x ratio at night is only 0.55 mol mol^{-1}, despite no NO_2 photolysis, because of

sustained NO emission and the slow rate of the $NO + O_3$ reaction (low ozone and low temperatures).

The opposite diurnal variation of NO_2 in summer reflects weaker daytime emission of NO_x and

stronger chemical loss as shown by the GEOS-Chem budget analysis. Even though the emission term

remains larger than the chemical loss term, there is also a negative transport term because upwind

250   emissions are much lower. Without the transport loss term, the NO_2 column in summer would still increase

over the course of the day. The chemical loss of NO_x peaks at 11-12 LT and then weakens, reflecting the

noon maximum of OH concentrations combined with the decreasing NO_2 concentration, and explaining the

slow recovery of the NO_2 column in the afternoon. The NO_2/NO_x ratio is higher in summer than in winter

and shows little variation during the daytime, reflecting the higher concentrations of O_3 and HO_2 radicals

255   offsetting the effect of NO_2 photolysis. The daytime NO_2/NO_x ratio averages 0.75 mol mol^{-1} in summer, as

compared to 0.5 mol mol^{-1} in winter, contributing to the seasonality of NO_2 seen from space.

Figure 5 shows the same as Figure 4 but for Seoul. The two Pandora stations show differences in

NO_2 columns, particularly in summer, as previously shown in Figure 2. They also show some differences in

diurnal variation, particularly in winter, which we similarly attribute to local effects such as different

260   emissions, wind speeds, and geography that cannot be resolved at 25-km resolution. The diurnal variations

of GEMS and GEOS-Chem agree to within the ranges defined by the Pandora data. NO_2 columns in winter

increase from 10 to 12 LT as in Beijing but then flatten in the afternoon, which we attribute in GEOS-

Chem to stronger winds. NO_2 columns in summer show an increase from 8 to 10 LT, unlike in Beijing,

10

because of larger emissions initially overwhelming the chemical loss term. There follows a decrease until

265   13-14 LT and a recovery in the later afternoon, similar to Beijing and driven by the same factors.

5.   Separating the influences of emission, chemistry, and transport

We showed in Section 4 that the diurnal variation of the NO_2 column observed by GEMS on the

urban scale reflects a balance between emission and transport in winter, and the added influence from

270   chemical loss in summer. This suggests that emission and chemical loss can be independently inferred from

the GEMS observations in winter and summer if the role of transport can be quantified. The transport term

can be represented with a CTM in an inversion framework (Cooper et al., 2017), but simple quantification

of the transport term on the urban scale can also be done from knowledge of the wind speed with a mass

balance approach (Jacob et al., 2016).

275   Figure 6 illustrates the sensitivity of the NO_2 diurnal variation to wind speed in the wintertime

GEMS observations over Seoul when chemical loss is a negligible term. Here the data are segregated by

hourly wind speed (6 m s^{-1}) at 850 hPa from NASA GEOS-FP meteorology. The diurnal variations are very

different at high and low wind speed, and consistent between GEMS and GEOS-Chem. At high wind

speed, the NO_2 column shows little diurnal variability because emission is balanced by transport. At low

280   wind speed, NO_2 accumulates throughout the day because the transport term is weaker and does not keep

up with emissions. But the transport term is not negligible even at low wind speed; for a 3 m s^{-1} wind, the

ventilation time scale for the 25-km urban domain is only 2 hours. This also explains why the transport

term remains important in summer (Figures 4 and 5), as the timescale for NO_x chemical loss is about 6

hours (Shah et al., 2020).

285   One can reduce the effect of transport by spatial averaging over a large domain, thereby increasing

the ventilation timescale. Figure 7 shows the average diurnal pattern of the NO_2 column observed by

GEMS and simulated by GEOS-Chem on the ≈150-km scale of the SMA (Figure 2) in winter and summer.

Again, the diurnal variations observed by GEMS and simulated by GEOS-Chem are consistent. NO_2

columns in winter increase over the course of the day in a more regular manner than on the 25-km urban

11

290   scale (Figure 5) because the transport loss term is steadier and responds mainly to the change in the NO_2 column. The chemical loss term is not negligible, unlike on the urban scale, because its timescale of 24 hours is comparable to that of transport.

       We see from Figure 7 that the transport term can be successfully marginalized on the scale of the SMA in summer because the chemical loss term is faster. The resulting SMA diurnal pattern of the total

295   NO_2 column is consistent with that of Seoul (Fig. 5b) but with a flatter shape and the early-afternoon minimum now driven mainly by chemistry. The amplitude is greatly dampened because emissions are five times weaker when averaged over the SMA regional domain, and because the chemical loss integrates over the residence time within the domain.

6. Conclusions

300   We used the GEOS-Chem model to interpret the diurnal variation of NO_2 columns observed from the GEMS geostationary instrument and Pandora ground-based spectrometers over East Asia in December-January-February (DJF) 2021/22 and June-July-August (JJA) 2022. This was motivated by the need to understand the unique information offered by hourly geostationary satellite observations on the budget of NO_x through the contributions of emissions, chemistry, and transport to the diurnal cycle of NO_2.

305   The GEOS-Chem model used in this work had previously shown successful simulation of the NO_2 vertical profile and its diurnal variation over Seoul in the KORUS-AQ aircraft campaign, resolving the diurnal dependence of the air mass factor (AMF) that contributes to the diurnal variation of NO_2 observed from space. Here we used the diagnostic budget capability in GEOS-Chem to isolate the contributions of NO_x emissions, chemistry, transport, and the NO_2/NO_x column ratio to the diurnal cycle of NO_2 columns.

310   We also updated NO_x emissions to 2022 including their diurnal variations. NO_x emissions for Beijing and Seoul are a factor of four higher in the daytime than at night, reflecting mobile and industrial sources, and show little variation during the daytime hours. We focused on simulation of the total atmospheric NO_2 column rather than the tropospheric column, taking advantage of the stratospheric capability in GEOS-

Chem, and to avoid errors in the definition of the tropopause. Diurnal variation of the NO_2 atmospheric

315 column is mainly determined by the planetary boundary layer (PBL) up to 3 km altitude.

We investigated the diurnal variation of the NO_2 column at the 25-km urban scale over Beijing and Seoul. GEMS, Pandora, and GEOS-Chem show similar variability and diurnal variations. NO_2 columns in winter increase over the course of the daytime hours, reflecting accumulation from high daytime emissions offset by loss from horizontal transport (flux divergence), and further enhanced by increase in the NO_2/NO_x

320 over the course of the day as ozone is entrained in the growing mixed layer. Chemical loss of NO_x in winter is too slow to play a significant role in the observed diurnal variation. In summer, by contrast, NO_2 columns decrease from 10 to 14 local time (LT) because of NO_x photochemical oxidation compounding the loss from transport. The NO_2 column would still increase throughout the day in summer as in winter were it not for the loss from transport.

325 Our results indicate that the diurnal variation of NO_2 column observed from geostationary orbit can be used to quantify urban NO_x emissions in winter, and chemical loss in summer, but the transport term must be accounted for. This can be done by simple mass balance using knowledge of the local wind speed or by an inversion with a full CTM.

We further examined the importance of transport for interpreting the diurnal variation in the GEMS

330 urban NO_2 data by segregating the Seoul data by wind speed. In winter, the low-wind GEMS data (< 6 m s$^-$
^{1}) show steady rise of NO_2 over the course of the day while the high-wind data (≥ 6 m s^{-1}) show flat diurnal variation, consistent with the GEOS-Chem the model. Transport plays an important role in the NO_x budget in both cases but cannot keep up with the high daytime emissions in the low-wind case.

We examined whether the role of transport in the diurnal variation of the urban NO_2 column could

335 be reduced by spatial averaging of the data over the 150-km regional scale of the Seoul Metropolitan Area (SMA). The SMA data in winter show a steady increase over the daytime hours due to emissions, but the transport term remains the major sink of NO_x. The SMA data in summer show negligible loss from

transport in daytime because chemical loss term is much faster, but the diurnal amplitude is weak because of diluted emissions and long residence times for the air over the regional domain.

340   Our conclusions regarding the interpretation of the diurnal variation of NO_2 columns observed by GEMS can be extended to other instruments of the geostationary air quality constellation, such as TEMPO over North America, launched in April 2023 and Sentinel-4 over Europe, scheduled for launch in 2024. This work further lays the groundwork for use of GEOS-Chem in inversions of the geostationary satellite data to infer NO_x emissions.

345 **Code Availability**

The model code used in this work is available at https://doi.org/10.5281/zenodo.5764874 (The International GEOS-Chem User Community, 2021).

Data availability

The GEMS L2 NO_2 v2.0 slant column data can be obtained with a request to the NIER GEMS team (NIER,
350 2023). The total NO_2 columns from Pandora are available from the Pandonia Global Network website (http://pandonia-global-network.org; PGN, 2023). The surface NO_2 data over China are available from https://quotsoft.net/air/ (MEE, 2023). The surface NO_2 data over South Korea are from AirKorea website (https://www.airkorea.or.kr; KEC, 2023). The Seoul hourly traffic count data is available from the Seoul Transport Operation and Information Services website (https://topis.seoul.go.kr/; TOPIS, 2023).

Author contribution

The original draft preparation was done by LHY, with review and editing by DJJ, KRT, JHC, HL, and JK.
360 DJJ contributed to project conceptualization. Modeling was done by LHY with additional support from HPL, NKC, SZ, VS, EB, XF, RMY, and DCP. The formal analysis was conducted by LHY with additional support from DJJ, RD, YJO, HC, JP, HLL, WJL, SK, EK, KRT, and JHC.

Competing Interests

Financial support

References

Bae, M., Yoo, C., Kim, H., and Kim, S.: Developing Temporal Allocation Profiles for Electric Generating Utilities based on the CleanSYS Real-time Emissions, J. Korean Soc. Atmos., 37, 338–354, https://doi.org/10.5572/KOSAE.2021.37.2.338, 2021.

Boersma, K. F., Jacob, D. J., Eskes, H. J., Pinder, R. W., Wang, J., and van der A, R. J.: Intercomparison of SCIAMACHY and OMI tropospheric NO_2 columns: Observing the diurnal evolution of chemistry and emissions from space, J. Geophys. Res., 113, 2007JD008816, https://doi.org/10.1029/2007JD008816, 2008.

Boersma, K. F., Jacob, D. J., Trainic, M., Rudich, Y., DeSmedt, I., Dirksen, R., and Eskes, H. J.: Validation of urban NO2 concentrations and their diurnal and seasonal variations observed from the SCIAMACHY and OMI sensors using in situ surface measurements in Israeli cities, Atmos. Chem. Phys., 9, 3867–3879, https://doi.org/10.5194/acp-9-3867-2009, 2009.

Chang, L.-S., Kim, D., Hong, H., Kim, D.-R., Yu, J.-A., Lee, K., Lee, H., Kim, D., Hong, J., Jo, H.-Y., and Kim, C.-H.: Evaluation of correlated Pandora column NO2 and in situ surface NO2 measurements during GMAP campaign, Atmos. Chem. Phys., 22, 10703–10720, https://doi.org/10.5194/acp-22-10703-2022, 2022.

Cheng, N., Li, Y., Sun, F., Chen, C., Wang, B., Li, Q., Wei, P., and Cheng, B.: Ground-Level NO2 in Urban Beijing: Trends, Distribution, and Effects of Emission Reduction Measures, Aerosol Air Qual. Res., 18, 343–356, https://doi.org/10.4209/aaqr.2017.02.0092, 2018.

Cooper, M., Martin, R. V., Padmanabhan, A., and Henze, D. K.: Comparing mass balance and adjoint methods for inverse modeling of nitrogen dioxide columns for global nitrogen oxide emissions, JGR Atmospheres, 122, 4718–4734, https://doi.org/10.1002/2016JD025985, 2017.

Crawford, J. H., Ahn, J.-Y., Al-Saadi, J., Chang, L., Emmons, L. K., Kim, J., Lee, G., Park, J.-H., Park, R. J., Woo, J. H., Song, C.-K., Hong, J.-H., Hong, Y.-D., Lefer, B. L., Lee, M., Lee, T., Kim, S., Min, K.-E., Yum, S. S., Shin, H. J., Kim, Y.-W., Choi, J.-S., Park, J.-S., Szykman, J. J., Long, R. W., Jordan, C. E., Simpson, I. J., Fried, A., Dibb, J. E., Cho, S., and Kim, Y. P.: The Korea–United States Air Quality (KORUS-AQ) field study, Elementa: Science of the Anthropocene, 9, 00163, https://doi.org/10.1525/elementa.2020.00163, 2021.

Ghude, S. D., Karumuri, R. K., Jena, C., Kulkarni, R., Pfister, G. G., Sajjan, V. S., Pithani, P., Debnath, S., Kumar, R., Upendra, B., Kulkarni, S. H., Lal, D. M., Vander A, R. J., and Mahajan, A. S.: What is driving the diurnal variation in tropospheric NO2 columns over a cluster of high emission thermal power plants in India?, Atmospheric Environment: X, 5, 100058, https://doi.org/10.1016/j.aeaoa.2019.100058, 2020.

Gulde, S. T., Kolm, M. G., Smith, D. J., Maurer, R., Courrèges-Lacoste, G. B., Sallusti, M., and Bagnasco, G.: Sentinel 4: a geostationary imaging UVN spectrometer for air quality monitoring: status of design, performance and development, in: International Conference on Space Optics — ICSO 2014, Tenerife, Spain, 17 November 2017, 1158–1166, https://doi.org/10.1117/12.2304099, 2017.

Herman, J., Cede, A., Spinei, E., Mount, G., Tzortziou, M., and Abuhassan, N.: NO_2 column amounts from ground-based Pandora and MFDOAS spectrometers using the direct-sun DOAS technique:

Intercomparisons and application to OMI validation, J. Geophys. Res., 114, 2009JD011848, https://doi.org/10.1029/2009JD011848, 2009.

Herman, J., Spinei, E., Fried, A., Kim, J., Kim, J., Kim, W., Cede, A., Abuhassan, N., and Segal-Rozenhaimer, M.: NO2 and HCHO measurements in Korea from 2012 to 2016 from Pandora Spectrometer Instruments compared with OMI retrievals and with aircraft measurements during the KORUS-AQ campaign, Atmos. Meas. Tech., 11, 4583-4603, https://doi.org/10.5194/amt-2018-56, 2018.

Judd, L. M., Al-Saadi, J. A., Szykman, J. J., Valin, L. C., Janz, S. J., Kowalewski, M. G., Eskes, H. J., Veefkind, J. P., Cede, A., Mueller, M., Gebetsberger, M., Swap, R., Pierce, R. B., Nowlan, C. R., Abad, G. G., Nehrir, A., and Williams, D.: Evaluating Sentinel-5P TROPOMI tropospheric NO2 column densities with airborne and Pandora spectrometers near New York City and Long Island Sound, Atmos. Meas. Tech., 13, 6113–6140, https://doi.org/10.5194/amt-13-6113-2020, 2020.

Jacob, D. J., Turner, A. J., Maasakkers, J. D., Sheng, J., Sun, K., Liu, X., Chance, K., Aben, I., McKeever, J., and Frankenberg, C.: Satellite observations of atmospheric methane and their value for quantifying methane emissions, Atmos. Chem. Phys., 16, 14371–14396, https://doi.org/10.5194/acp-16-14371-2016, 2016.

Kanaya, Y., Irie, H., Takashima, H., Iwabuchi, H., Akimoto, H., Sudo, K., Gu, M., Chong, J., Kim, Y. J., Lee, H., Li, A., Si, F., Xu, J., Xie, P.-H., Liu, W.-Q., Dzhola, A., Postylyakov, O., Ivanov, V., Grechko, E., Terpugova, S., and Panchenko, M.: Long-term MAX-DOAS network observations of NO2; in Russia and Asia (MADRAS) during the period 2007–2012: instrumentation, elucidation of climatology, and comparisons with OMI satellite observations and global model simulations, Atmos. Chem. Phys., 14, 7909–7927, https://doi.org/10.5194/acp-14-7909-2014, 2014.

KEC: The Korea Environment Corporation NO2 dataset in South Korea - AirKorea [data set], https://www.airkorea.or.kr, 2023.

Kendrick, C. M., Koonce, P., and George, L. A.: Diurnal and seasonal variations of NO, NO2 and PM2.5 mass as a function of traffic volumes alongside an urban arterial, Atmos. Environ., 122, 133–141, https://doi.org/10.1016/j.atmosenv.2015.09.019, 2015.

Kim, H. C., Kim, S., Lee, S.-H., Kim, B.-U., and Lee, P.: Fine-Scale Columnar and Surface NOx Concentrations over South Korea: Comparison of Surface Monitors, TROPOMI, CMAQ and CAPSS Inventory, Atmosphere, 11, 101, https://doi.org/10.3390/atmos11010101, 2020.

Kim, J., Kim, J., Cho, H.-K., Herman, J., Park, S. S., Lim, H. K., Kim, J.-H., Miyagawa, K., and Lee, Y. G.: Intercomparison of total column ozone data from the Pandora spectrophotometer with Dobson, Brewer, and OMI measurements over Seoul, Korea, Atmos. Meas. Tech., 10, 3661–3676, https://doi.org/10.5194/amt-10-3661-2017, 2017.

Kim, J., Jeong, U., Ahn, M.-H., Kim, J. H., Park, R. J., Lee, H., Song, C. H., Choi, Y.-S., Lee, K.-H., Yoo, J.-M., Jeong, M.-J., Park, S. K., Lee, K.-M., Song, C.-K., Kim, S.-W., Kim, Y. J., Kim, S.-W., Kim, M., Go, S., Liu, X., Chance, K., Chan Miller, C., Al-Saadi, J., Veihelmann, B., Bhartia, P. K., Torres, O., Abad, G. G., Haffner, D. P., Ko, D. H., Lee, S. H., Woo, J.-H., Chong, H., Park, S. S., Nicks, D., Choi, W. J., Moon, K.-J., Cho, A., Yoon, J., Kim, S., Hong, H., Lee, K., Lee, H., Lee, S., Choi, M., Veefkind, P., Levelt, P. F., Edwards, D. P., Kang, M., Eo, M., Bak, J., Baek, K., Kwon, H.-A., Yang, J., Park, J., Han, K. M., Kim, B.-R., Shin, H.-W., Choi, H., Lee, E., Chong, J., Cha, Y., Koo, J.-H., Irie, H., Hayashida, S., Kasai, Y., Kanaya, Y., Liu, C., Lin, J., Crawford, J. H., Carmichael, G. R., Newchurch, M. J., Lefer, B. L., Herman, J. R., Swap, R. J., Lau, A. K. H., Kurosu, T. P., Jaross, G., Ahlers, B., Dobber, M., McElroy, C. T., and Choi, Y.: New Era of Air Quality Monitoring from Space: Geostationary Environment Monitoring Spectrometer (GEMS), B. Am. Meteorol. Soc., 101, E1–E22, https://doi.org/10.1175/BAMS-D-18-0013.1, 2020.

Kim, M.-H., Yeo, H., Park, S., Park, D.-H., Omar, A., Nishizawa, T., Shimizu, A., and Kim, S.-W.: Assessing CALIOP-Derived Planetary Boundary Layer Height Using Ground-Based Lidar, Remote Sens., 13, 1496, https://doi.org/10.3390/rs13081496, 2021.

Kim, S., Kim, D., Hong, H., Chang, L.-S., Lee, H., Kim, D.-R., Kim, D., Yu, J.-A., Lee, D., Jeong, U., Song, C.-K., Kim, S.-W., Park, S. S., Kim, J., Hanisco, T. F., Park, J., Choi, W., and Lee, K.: First-time comparison between NO2 vertical columns from Geostationary Environmental Monitoring Spectrometer (GEMS) and Pandora measurements, Atmos. Meas. Tech., 16, 3959-3972, https://doi.org/10.5194/amt-2023-11, 2023.

Lee, H., Park, J., and Hyunkee, H.: Geostationary Environment Monitoring Spectrometer (GEMS) User's Guide - Nitrogen Dioxide, The National Institute of Environmental Research, Republic of Korea, https://nesc.nier.go.kr/ko/html/satellite/guide/guide.do, 2020.

Liu, M., Lin, J., Wang, Y., Sun, Y., Zheng, B., Shao, J., Chen, L., Zheng, Y., Chen, J., Fu, T.-M., Yan, Y., Zhang, Q., and Wu, Z.: Spatiotemporal variability of NO2and PM2.5 over Eastern China: observational and model analyses with a novel statistical method, Atmos. Chem. Phys., 18, 12933–12952, https://doi.org/10.5194/acp-18-12933-2018, 2018.

Liu, O., Li, Z., Lin, Y., Fan, C., Zhang, Y., Li, K., Zhang, P., Wei, Y., Chen, T., Dong, J., and de Leeuw, G.: Evaluation of the first year of Pandora NO2 measurements over Beijing and application to satellite validation, Atmos. Meas. Tech. Discuss., 1-32, https://doi.org/10.5194/amt-2023-177, 2023.

Liu, X., Gao, X., Wu, X., Yu, W., Chen, L., Ni, R., Zhao, Y., Duan, H., Zhao, F., Chen, L., Gao, S., Xu, K., Lin, J., and Ku, A. Y.: Updated Hourly Emissions Factors for Chinese Power Plants Showing the Impact of Widespread Ultralow Emissions Technology Deployment, Environ. Sci. Technol., 53, 2570–2578, https://doi.org/10.1021/acs.est.8b07241, 2019.

NIER: The National Institute of Environmental Research of Republic of South Korea - GEMS dataset [data set], https://nesc.nier.go.kr/, 2023.

Martin, R. V., Chance, K., Jacob, D. J., Kurosu, T. P., Spurr, R. J. D., Bucsela, E., Gleason, J. F., Palmer, P. I., Bey, I., Fiore, A. M., Li, Q., Yantosca, R. M., and Koelemeijer, R. B. A.: An improved retrieval of tropospheric nitrogen dioxide from GOME, J. Geophys. Res., 107, https://doi.org/10.1029/2001JD001027, 2002.

MEE: The Ministry of Ecology and Environment NO$_2$ dataset in China, MEE [data set], https://quotsoft.net/air/, 2023.

Miao, R., Chen, Q., Zheng, Y., Cheng, X., Sun, Y., Palmer, P. I., Shrivastava, M., Guo, J., Zhang, Q., Liu, Y., Tan, Z., Ma, X., Chen, S., Zeng, L., Lu, K., and Zhang, Y.: Model bias in simulating major chemical components of PM2.5 in China, Atmos. Chem. Phys., 20, 12265–12284, https://doi.org/10.5194/acp-20-12265-2020, 2020.

Moutinho, J. L., Liang, D., Golan, R., Sarnat, S. E., Weber, R., Sarnat, J. A., and Russell, A. G.: Near-road vehicle emissions air quality monitoring for exposure modeling, Atmos. Environ., 224, 117318, https://doi.org/10.1016/j.atmosenv.2020.117318, 2020.

Palmer, P. I., Jacob, D. J., Chance, K., Martin, R. V., Spurr, R. J. D., Kurosu, T. P., Bey, I., Yantosca, R., Fiore, A., and Li, Q.: Air mass factor formulation for spectroscopic measurements from satellites: Application to formaldehyde retrievals from the Global Ozone Monitoring Experiment, J. Geophys. Res., 106, 14539–14550, https://doi.org/10.1029/2000JD900772, 2001.

Park, R. J. and Kwon, H.-A.: Algorithm Theoretical Basis Document - VOC (HCHO/CHOCHO) Retrieval Algorithm, The National Institute of Environmental Research, Republic of Korea, https://nesc.nier.go.kr/en/html/satellite/doc/doc.do, 2020.

Park, R. J., Oak, Y. J., Emmons, L. K., Kim, C.-H., Pfister, G. G., Carmichael, G. R., Saide, P. E., Cho, S.-Y., Kim, S., Woo, J.-H., Crawford, J. H., Gaubert, B., Lee, H.-J., Park, S.-Y., Jo, Y.-J., Gao, M., Tang, B., Stanier, C. O., Shin, S. S., Park, H. Y., Bae, C., and Kim, E.: Multi-model intercomparisons of air quality simulations for the KORUS-AQ campaign, Elementa: Science of the Anthropocene, 9, 00139, https://doi.org/10.1525/elementa.2021.00139, 2021.

Park, S., Kim, S.-W., Park, M.-S., and Song, C.-K.: Measurement of Planetary Boundary Layer Winds with Scanning Doppler Lidar, Remote Sens., 10, 1261, https://doi.org/10.3390/rs10081261, 2018.

505   Penn, E. and Holloway, T.: Evaluating current satellite capability to observe diurnal change in nitrogen oxides in preparation for geostationary satellite missions, Environ. Res. Lett., 15, 034038, https://doi.org/10.1088/1748-9326/ab6b36, 2020.

PGN: Pandonia Global Network (PGN) data archive [data set], http://data.pandonia-global-network.org/, 2023.

510   Seo, S., Kim, S.-W., Kim, K.-M., Lamsal, L. N., and Jin, H.: Reductions in NO_2 concentrations in Seoul, South Korea detected from space and ground-based monitors prior to and during the COVID-19 pandemic, Environ. Res. Commun., 3, 051005, https://doi.org/10.1088/2515-7620/abed92, 2021.

Shah, V., Jacob, D. J., Li, K., Silvern, R. F., Zhai, S., Liu, M., Lin, J., and Zhang, Q.: Effect of changing NO2 lifetime on the seasonality and long-term trends of satellite-observed tropospheric NO2

515   columns over China, Atmos. Chem. Phys., 20, 1483–1495, https://doi.org/10.5194/acp-20-1483-2020, 2020.

The International GEOS-Chem User Community: geoschem/GC-Classic: GEOS-Chem 13.3.4 (13.3.4), Zenodo [code], https://doi.org/10.5281/zenodo.5764874, 2021.

TOPIS: Seoul Transport Operation and Information Services (TOPIS) Seoul traffic count data [data set],
520   https://topis.seoul.go.kr/, 2023.

Verhoelst, T., Compernolle, S., Pinardi, G., Lambert, J.-C., Eskes, H. J., Eichmann, K.-U., Fjæraa, A. M., Granville, J., Niemeijer, S., Cede, A., Tiefengraber, M., Hendrick, F., Pazmiño, A., Bais, A., Bazureau, A., Boersma, K. F., Bognar, K., Dehn, A., Donner, S., Elokhov, A., Gebetsberger, M., Goutail, F., Grutter de la Mora, M., Gruzdev, A., Gratsea, M., Hansen, G. H., Irie, H., Jepsen, N.,
525   Kanaya, Y., Karagkiozidis, D., Kivi, R., Kreher, K., Levelt, P. F., Liu, C., Müller, M., Navarro Comas, M., Piters, A. J. M., Pommereau, J.-P., Portafaix, T., Prados-Roman, C., Puentedura, O., Querel, R., Remmers, J., Richter, A., Rimmer, J., Rivera Cárdenas, C., Saavedra de Miguel, L., Sinyakov, V. P., Stremme, W., Strong, K., Van Roozendael, M., Veefkind, J. P., Wagner, T., Wittrock, F., Yela González, M., and Zehner, C.: Ground-based validation of the Copernicus
530   Sentinel-5P TROPOMI NO2 measurements with the NDACC ZSL-DOAS, MAX-DOAS and Pandonia global networks, Atmos. Meas. Tech., 14, 481–510, https://doi.org/10.5194/amt-14-481-2021, 2021.

Woo, J.-H., Kim, Y., Kim, H.-K., Choi, K.-C., Eum, J.-H., Lee, J.-B., Lim, J.-H., Kim, J., and Seong, M.: Development of the CREATE Inventory in Support of Integrated Climate and Air Quality Modeling
535   for Asia, Sustainability, 12, https://doi.org/10.3390/su12197930, 2020.

Yang, L. H., Jacob, D. J., Colombi, N. K., Zhai, S., Bates, K. H., Shah, V., Beaudry, E., Yantosca, R. M., Lin, H., Brewer, J. F., Chong, H., Travis, K. R., Crawford, J. H., Lamsal, L. N., Koo, J.-H., and Kim, J.: Tropospheric NO_2 vertical profiles over South Korea and their relation to oxidant chemistry: implications for geostationary satellite retrievals and the observation of NO_2 diurnal
540   variation from space, Atmos. Chem. Phys., 23, 2465–2481, https://doi.org/10.5194/acp-23-2465-2023, 2023.

Zheng, B., Zhang, Q., Geng, G., Chen, C., Shi, Q., Cui, M., Lei, Y., and He, K.: Changes in China's anthropogenic emissions and air quality during the COVID-19 pandemic in 2020, Earth Syst. Sci. Data, 13, 2895–2907, https://doi.org/10.5194/essd-13-2895-2021, 2021.

545   Zoogman, P., Liu, X., Suleiman, R. M., Pennington, W. F., Flittner, D. E., Al-Saadi, J. A., Hilton, B. B., Nicks, D. K., Newchurch, M. J., Carr, J. L., Janz, S. J., Andraschko, M. R., Arola, A., Baker, B. D., Canova, B. P., Chan Miller, C., Cohen, R. C., Davis, J. E., Dussault, M. E., Edwards, D. P., Fishman, J., Ghulam, A., González Abad, G., Grutter, M., Herman, J. R., Houck, J., Jacob, D. J., Joiner, J., Kerridge, B. J., Kim, J., Krotkov, N. A., Lamsal, L., Li, C., Lindfors, A., Martin, R. V.,
550   McElroy, C. T., McLinden, C., Natraj, V., Neil, D. O., Nowlan, C. R., O′Sullivan, E. J., Palmer, P. I., Pierce, R. B., Pippin, M. R., Saiz-Lopez, A., Spurr, R. J. D., Szykman, J. J., Torres, O., Veefkind, J. P., Veihelmann, B., Wang, H., Wang, J., and Chance, K.: Tropospheric emissions: Monitoring of pollution (TEMPO), J. Quant. Spectrosc. Radiat. Transf., 186, 17–39, https://doi.org/10.1016/j.jqsrt.2016.05.008, 2017.
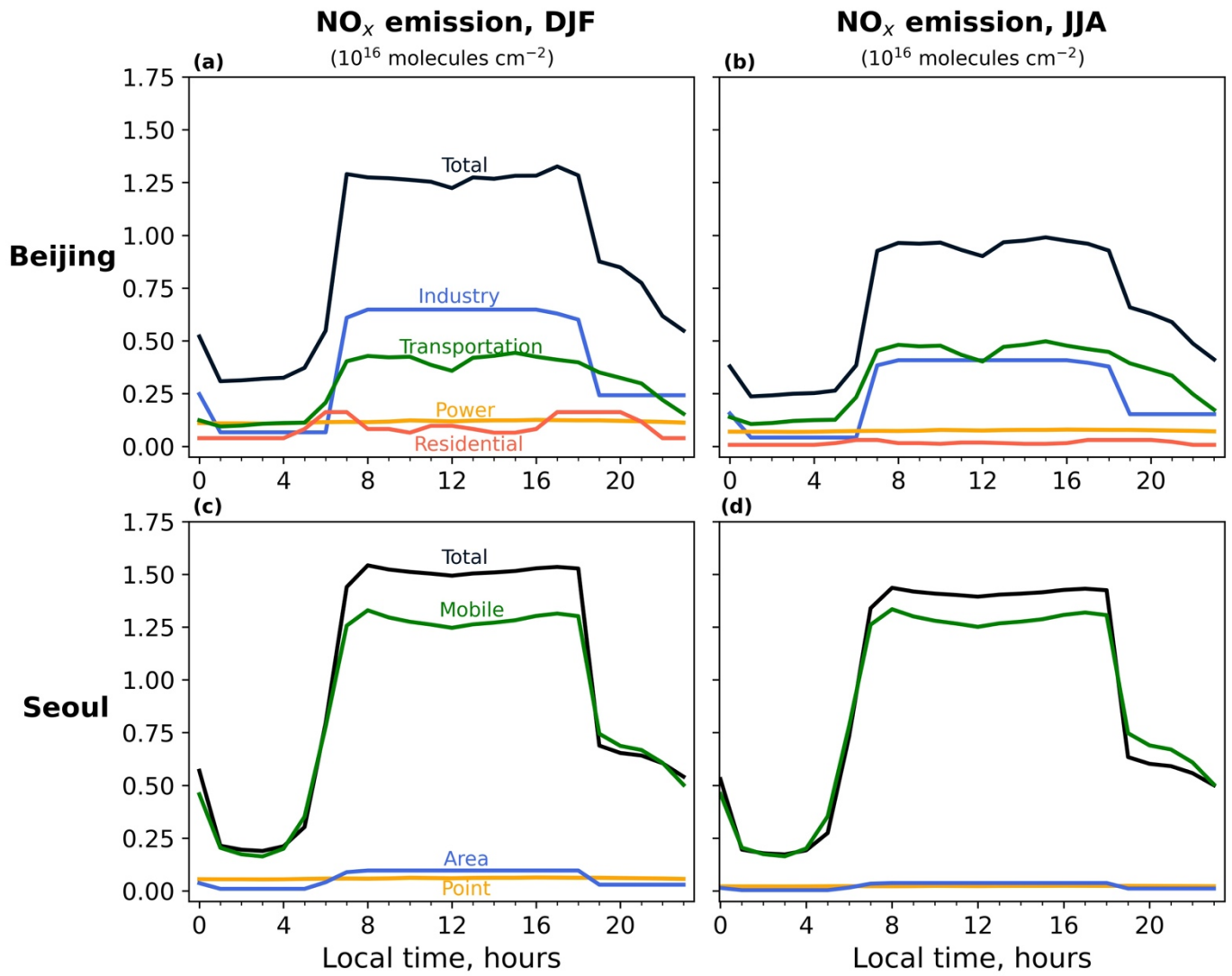
Figure 1. Diurnal variation of NO$_x$ emissions in Beijing and Seoul for DJF 2021/2022 and JJA 2022. Local time is Chinese Standard Time (CST) for Beijing and Korean Standard Time (KST) for Seoul. Solar noon is at 12:08 – 12:27 CST in Beijing and 12:21 – 12:45 KST in Seoul. Values are for the white boxes in Figure 2. Different colors represent different sectors, and the black line shows the total emission.
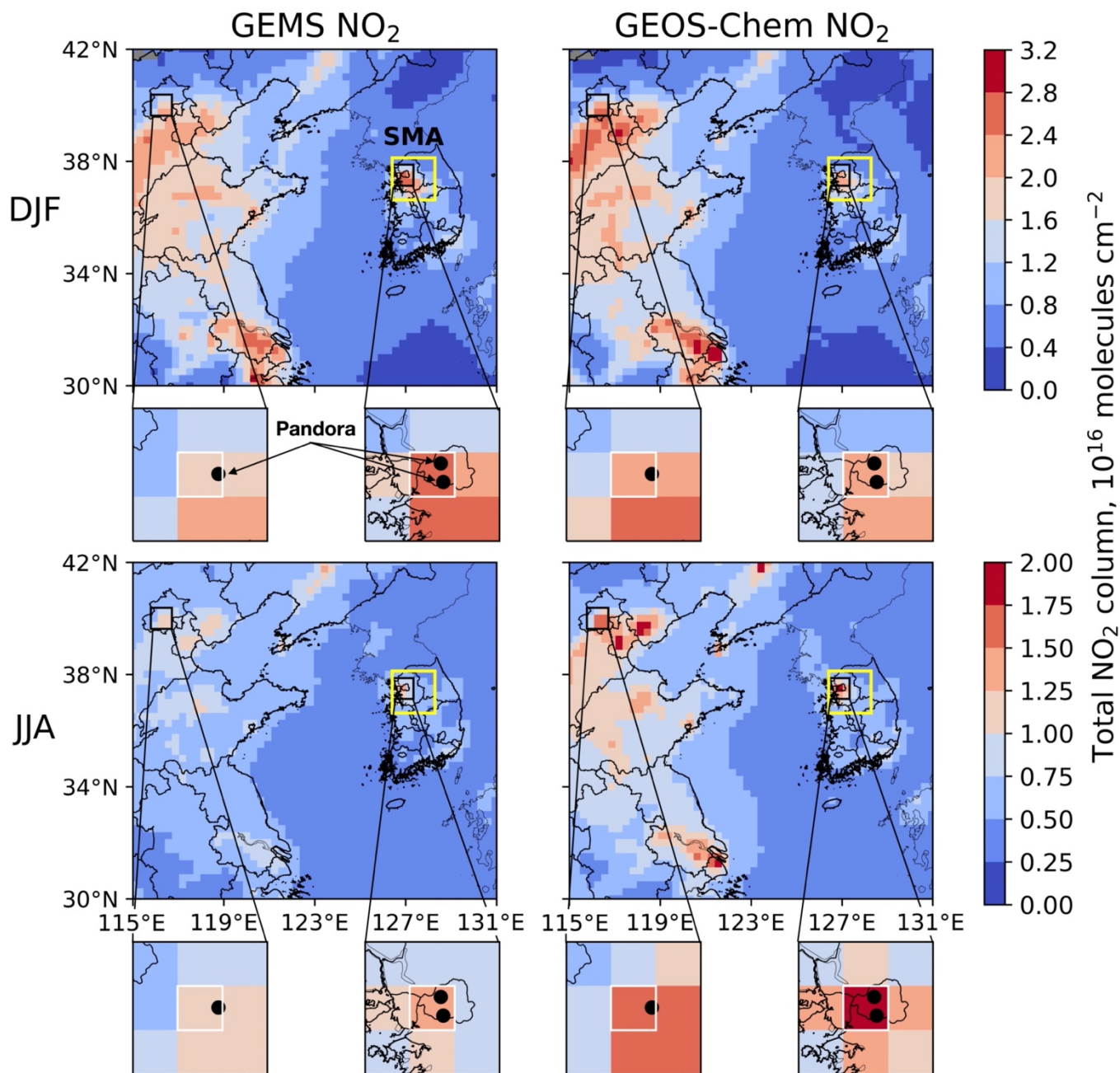
Figure 2. Total NO$_2$ columns over East Asia retrieved by GEMS and simulated by GEOS-Chem. The data are 3-month averages for December-July-February (DJF) 2021/22 and June-July-August (JJA) 2022 on the 0.25° × 0.3125° GEOS-Chem nested grid. The yellow rectangle delineates the Seoul Metropolitan Area (SMA; 36.6-38.1°N, 126.4-128.3°E). The zoomed-in plots show Beijing and Seoul, and the white boxes are the 0.25° × 0.3125° urban cores where the Pandora stations are located (black circles). Scales are different for DJF and JJA.
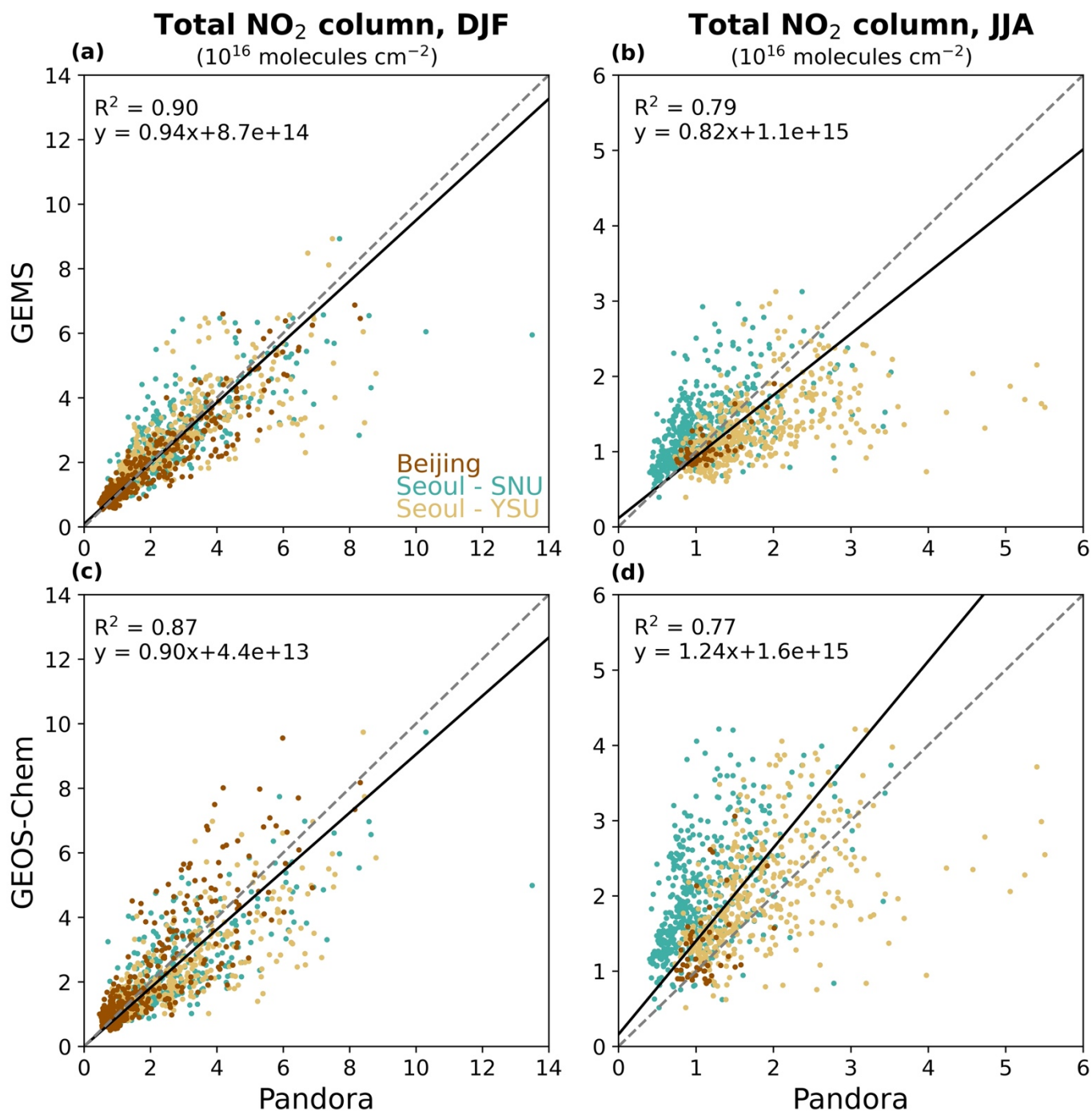
Figure 3. Intercomparison of GEOS-Chem, GEMS, and Pandora NO_2 columns for the Pandora sites in Beijing and Seoul. The Figure shows scatterplots of daytime hourly data for DJF 2021/2022 and JJA 2022. GEMS is mapped on the 0.25° × 0.3125° GEOS-Chem grid. Coefficients of determination (R^2) and reduced-major axis linear regressions are shown. The 1:1 line is dashed. The Beijing Pandora site has limited observations in JJA.
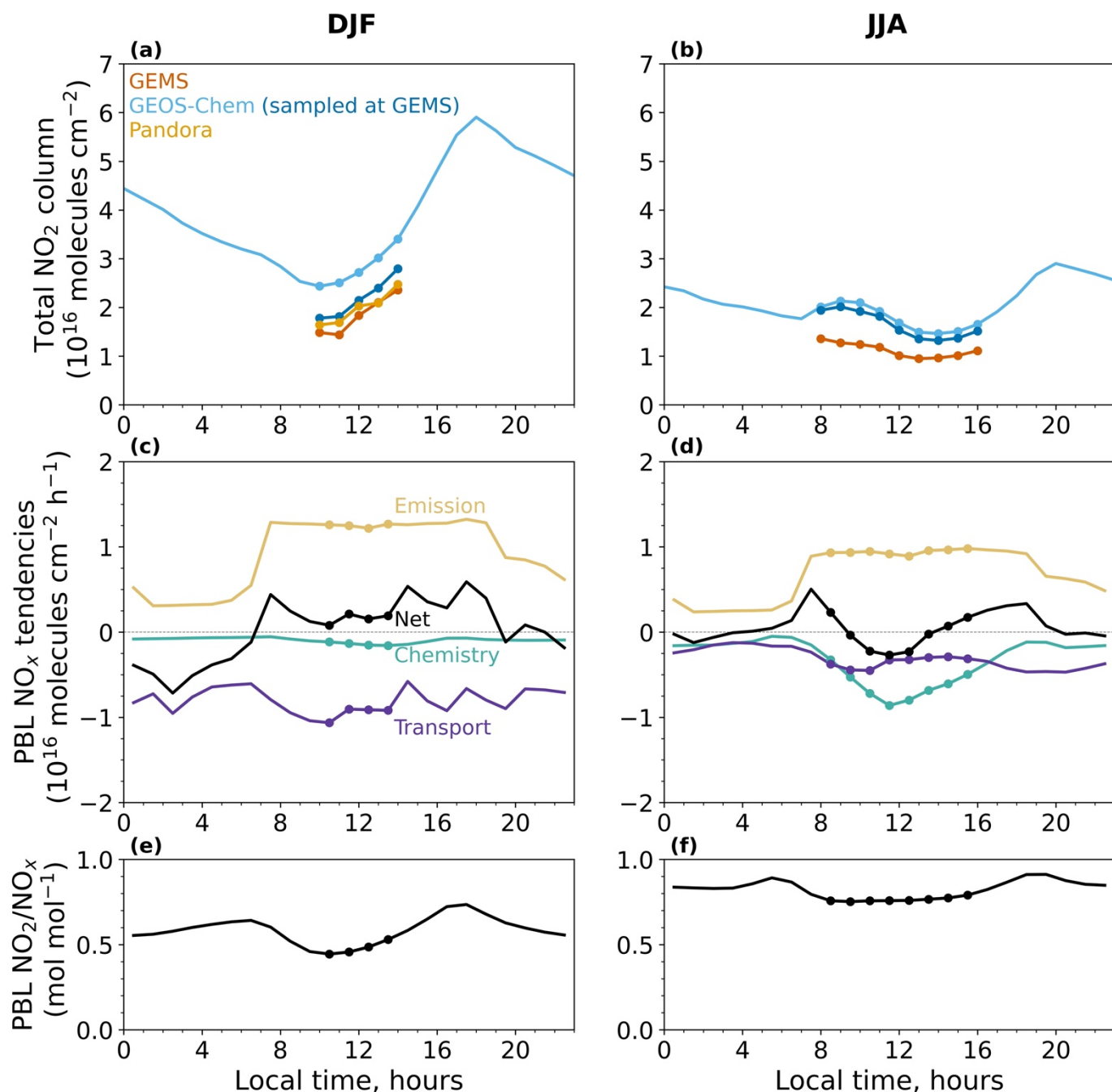
21

Figure 4. Diurnal variation of total NO₂ column and driving processes in Beijing. The first row shows the average NO₂ columns observed by GEMS and Pandora, and simulated by GEOS-Chem, in DJF 2021/22 and JJA 2022 for the 0.25° × 0.3125° GEOS-Chem grid cell in the urban core where the Pandora station is located (white box in Figure 2). GEMS observations are available for the hours indicated by symbols. GEOS-Chem results for the full diurnal cycle are shown as averages for all days and for the subset of days when GEMS data are available (generally limited by cloud cover). Pandora data are not shown for JJA due to a limited number of observations (Figure 3). The second row shows the hourly tendencies in the GEOS-Chem NOₓ budget (averaged for all days) for the planetary boundary layer (PBL) conservatively defined as extending up to 3 km altitude. The tendencies describe the contributions from individual processes to the NOₓ budget as given by Eq. (3), with NOₓ defined as $NO_x \equiv NO + NO_2 + NO_3 + 2N_2O_5 + HONO + HNO_4 + ClNO_2$. The third row shows the PBL NO₂/NOₓ column molar ratio in GEOS-Chem.

580

585

Seoul, South Korea

DJF

(a)

GEMS
GEOS-Chem (sampled at GEMS)
Pandora-SNU
Pandora-YSU

Total NO$_2$ column
(10^{16} molecules cm^{-2})

JJA

(b)

(c)

Emission

Chemistry

Net

Transport

PBL NO$_x$ tendencies
(10^{16} molecules cm^{-2} h^{-1})

(d)

(e)

PBL NO$_2$/NO$_x$
(mol mol^{-1})

Local time, hours

(f)

Local time, hours
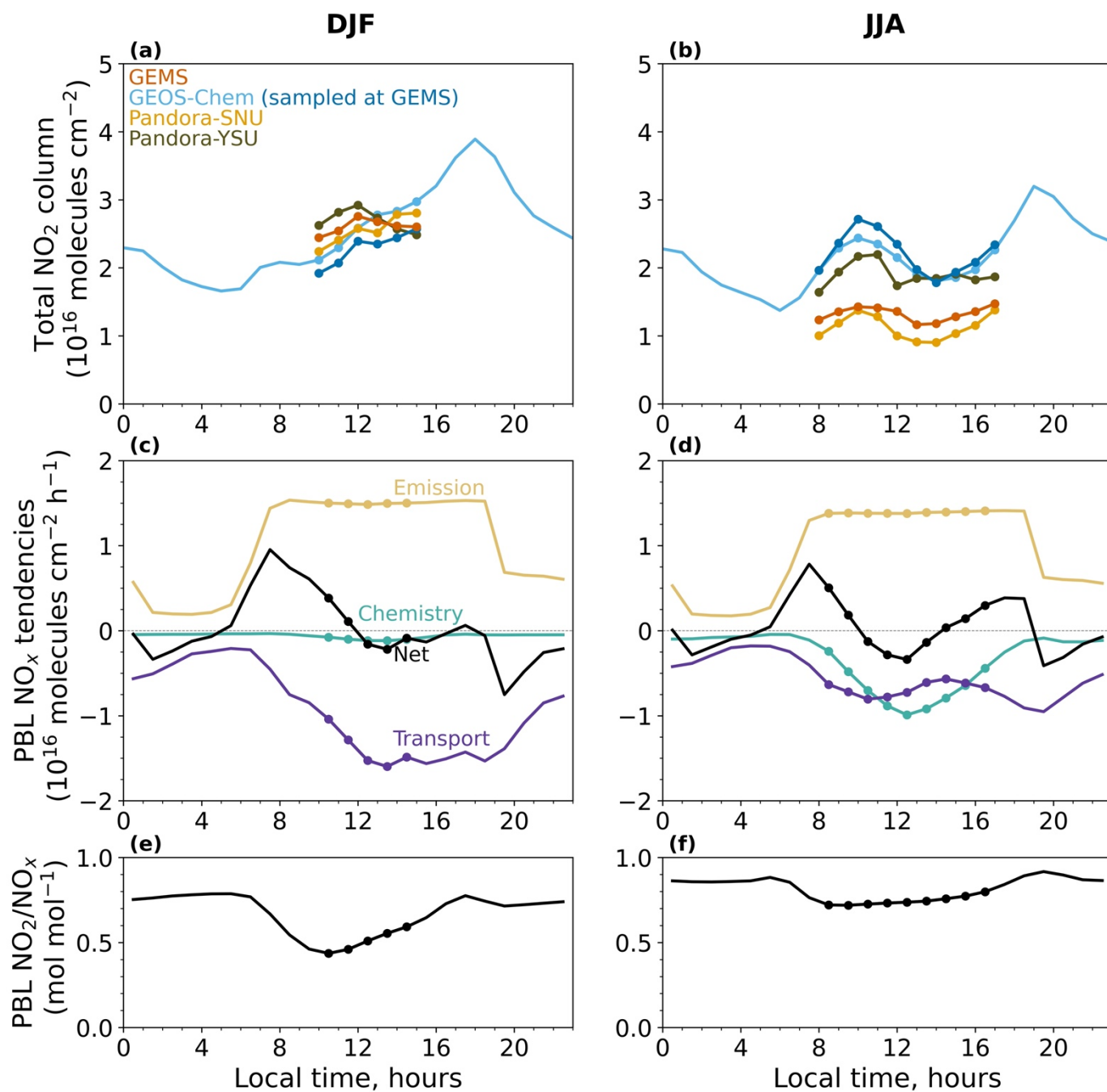
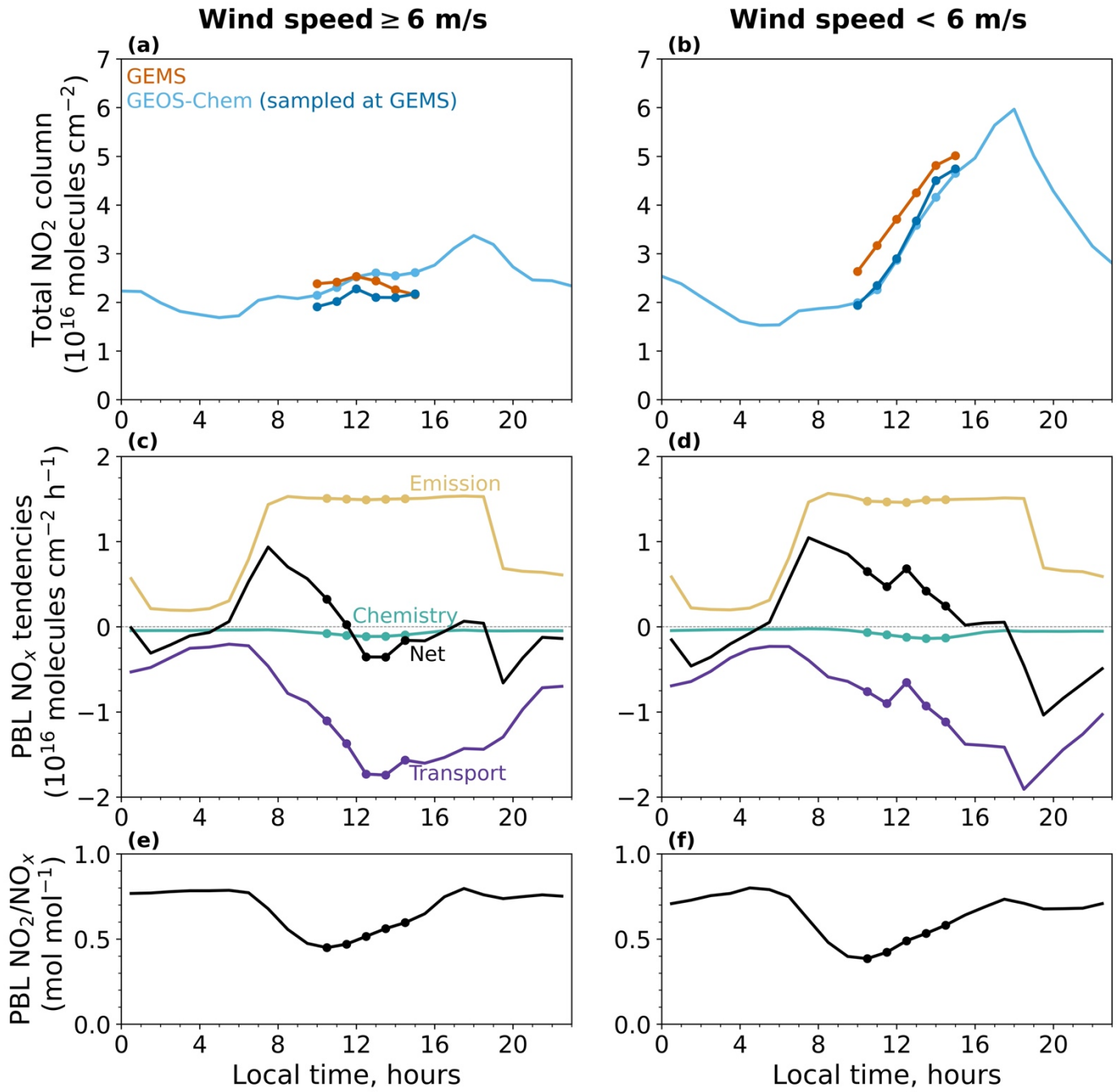**Figure 5.** Same as Figure 4 but for Seoul.

23

Figure 6. Same as Figure 4 but for DJF 2021/22 in Seoul with data segregated by wind speed. Segregation threshold is 6 m s⁻¹ for the 850 hPa hourly wind speed in the NASA GEOS-FP meteorological data used as input to GEOS-Chem.
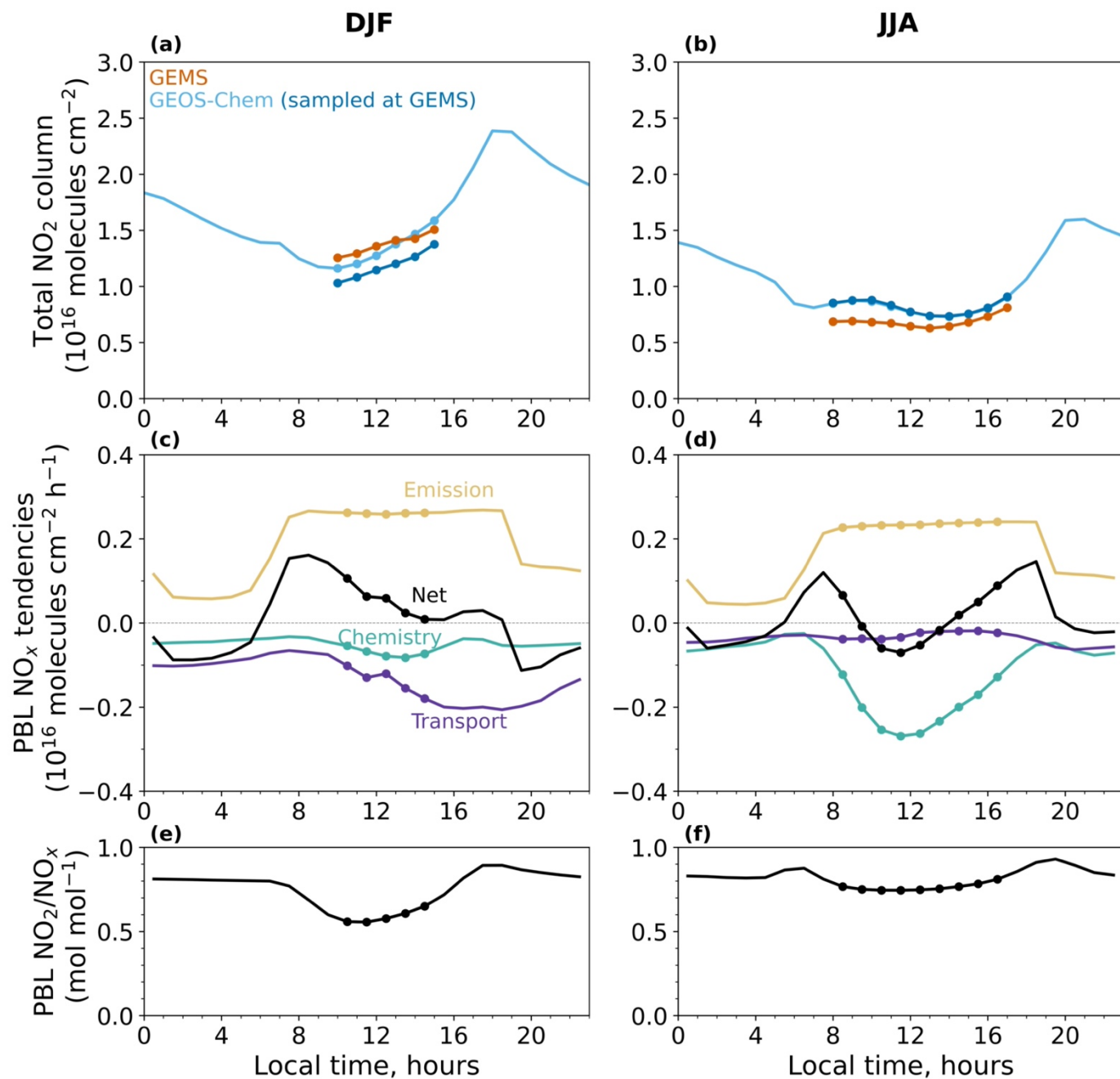
Figure 7. Same as for Figure 4 but for the Seoul Metropolitan Area (SMA; 36.6-38.1°N, 126.4-128.3°E) corresponding to the yellow box in Figure 2.

605